JOURNAL OF INFORMATION SCIENCE AND ENGINEERING 34, 701-720 (2018)
DOI: 10.6688/JISE.201805_34(3).0008

Using a Hybrid of Morphological Operation and Neuro-Fuzzy Filter for Transmission Map Refinement and Halation Elimination in Weather Degraded Images*

HSUEH-YI LIN[1], CHENG-JIAN LIN[1,+] AND MEI-LING HUANG[2]
[1]*Department of Computer Science and Information Engineering*
[2]*Department of Industrial Engineering and Management*
National Chin-Yi University of Technology
Taichung City, 411 Taiwan

For photographs taken in outdoor environments, the air medium causes light attenuation, which reduces image quality; this effect is particularly obvious in hazy environments. To eliminate the hazy effect in images and improve the image quality, the present study proposes an efficient hybrid method. The proposed fuzzy estimator was adopted to estimate variations in light attenuation, and morphological erosion and a neuro-fuzzy filter proposed by this study were employed to refine the transmission map and eliminate the halation. Finally, an estimated mean value for atmospheric light was applied to calculate the color vector of atmospheric light to eliminate the color cast. Experimental results indicate that the proposed hybrid method is superior to other dehazing methods.

Keywords: dehazing, fuzzy estimator, neuro-fuzzy filter, learning algorithm, transmission map, halation

1. INTRODUCTION

When a computer vision system is used in an outdoor environment, fog, smoke, haze, and other natural phenomena must be considered, because such phenomena can reduce visibility and image quality, causing errors in the image system or even rendering it ineffective. Many studies [1-4] have attempted to overcome the impacts of climate factors on image quality by applying physical modeling, correct color casting, and contrast enhancement.

In recent studies, two types of dehazing methods have been proposed: multiple image processing [1-5] and single image processing [6-12]. Regarding the multiple image processing methods, many researchers [1-5] have employed light polarization by rotating a polarizer on a camera and taking many hazy photos of the same scene for analysis.

For single image processing methods, Fattle [6] supposed that the transmission factor is not relevant to the surface color, and therefore, utilized independent component analysis (ICA) to estimate the transmission factor of light and the Markov random field to estimate the real color of the scene. However, because of the lengthy calculation time and insufficient color information, this approach is unsuitable for heavy haze environments. Tan *et al.* [7] summed the adjacent gradients of single pixels of an image to improve the contrast. In order to achieve dehazing by maximizing the image contrast, the

Received October 27, 2016; revised January 18 & March 27, 2017; accepted April 23, 2017.
Communicated by Chia-Feng Juang.
+ Correspondence author: cjlin@ncut.edu.tw
* This work was supported in part by the Ministry of Science and Technology, Taiwan, under Grant MOST 105-2221-E-167-028.

Markov random field was used to estimate the color of atmospheric light to improve color attenuation. However, this method presented problems with color super-saturation and halation. Tarel *et al.* [8] supposed that white balance could be used to correct the color deviation when the haze is pure white, and hence proposed a fast median filter to resolve the halation effect. Although that method is efficient, it cannot be used to eliminate peripheral halation. He *et al.* [9] proposed estimating the atmospheric light and transmission factor of a hazy image on the basis of dark channel prior. Thus, the scene radiance recovery resulted in block features and obvious halation in the boundary area of the image. To overcome the considerable computation time required by the refined transmission map method using soft matting in [9], He *et al.* [10] adopted a guided filter to refine the transmission map to avoid the halo problem. Meng *et al.* [11] proposed an effective regularization dehazing method for restoring haze-free images by investigating the inherent boundary constraint. This constraint, combined with a weighted L_1-norm based contextual regularization, is modeled into an optimization problem to estimate the unknown scene transmission. In order to eliminate halo artifacts, Wang *et al.* [15, 16] proposed a weighted ratio for the refinement of the transmission map. Two transmission planes are calculated by using mask sizes of 7×7 and 1×1. The 7×7 mask provides a window transmission map (WTM), whereas the 1×1 mask presents a pixel transmission map (PTM).

Recently, machine learning method is widely applied on various imaging techniques [17-25]. Fuzzy inference is based on how humans think and express word ambiguity, whereas neural networks emulate the learning abilities and organizational structure of the human brain. Images contain many uncertain factors that can affect image processing results. To define such uncertain factors, some researchers have employed fuzzy logic to solve various imaging problems, such as image filtering [17], image recognition [18], and image enhancement [19]. Likewise, neural network image learning features are applied on the fields of scene radiance recovery [20], image compression [21], human face detection [22, 23], and image classification [24].

The present study focused on the single-image dehazing problem. Although many dehazing methods [6-14] may achieve image dehazing problems, the dehazing effect, halation, and color casting continue to pose problems in this field. To resolve these problems, the present study proposes an efficient hybrid method for single-image haze removal. In the proposed method, a fuzzy estimator is adopted to estimate the variations in light attenuation, whereas morphological erosion and a neurofuzzy filter (NFF) proposed by this study are employed to eliminate the halation and optimize the transmission map refinement. An estimated mean value for atmospheric light is used to calculate the color vector of atmospheric light to eliminate color cast. The contributions of this study are as follows:

- The proposed fuzzy estimator can estimate the transmission map
- Morphological erosion and the proposed NFF can eliminate halation
- Color casting is resolved by calculating the atmospheric color vector on the basis of the mean value of the brightest 1% of atmospheric light

2. PREVIOUS AND RELATED WORK

A physical model of light creating a hazy image [1-4] can be expressed as

$$I(x) = J(x)\times t(x)+A\times(1- t(x)). \quad (1)$$

Here I is the hazy image captured by the lens; J is dehazed image; A is the atmospheric light; $t(x)$ is the transmission map; and x is the coordinate point. In Eq. (1), the mathematical expression $J(x)\times t(x)$ presents the direct attenuation, which is the attenuation when the scene radiance interacts with particles during transmission. The expression $A\times(1- t(x))$ shows the real color cast of the scene due to the scattering of atmospheric light. According to the Lambert-Beer's Law [2], when light propagates through air, the light at the atmospheric coordinate point is exponentially attenuated relative to the transmission distance, as shown in the following equation:

$$t(x) = e^{-\beta d(x)}. \quad (2)$$

Where $d(x)$ indicates the depth value of the atmospheric coordinate point x, and β denotes the attenuation coefficient. The vector spaces of hazy image I, dehazing image J, and atmospheric light A, have their own color channel intensity. For a given pixel, the three color channels will have the same transmission factor; but for an entire image, the transmission factor of each pixel point is quite different.

The general image dehazing process is shown in Fig. 1. First, the input image is used to estimate the transmission map; then transmission refinement is employed to overcome the halation. Next, the color cast is solved by the atmospheric light estimation. Finally, the scene radiance recovery result is produced.

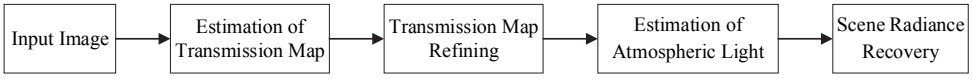

Fig. 1. The general image dehazing process.

3. THE PROPOSED IMAGE DEHAZING METHOD

This study developed an efficient hybrid method for dehazing images. In the proposed method, a fuzzy estimator is first used to estimate the transmission map. Because the proposed transmission map estimation causes a halation phenomenon, morphological erosion and the proposed NFF are then used to refine the transmission map and eliminate the halation. When scene radiance is recovered using the brightest pixel as the estimate for atmospheric light, color casting occurs; to improve the radiance recovery, the mean estimated value of atmospheric light is used to enhance the scene radiance recovery. The proposed hybrid method for dehazing is shown in Fig. 2.

3.1 Transmission Map Estimation Using a Fuzzy Estimator

Fig. 3 shows the basic architecture of a fuzzy logic system. The fuzzifier transforms crisp data into suitable linguistic value. The fuzzy rule base stores the empirical knowledge of the domain experts. The inference engine, which is the kernel of a fuzzy logic system, performs approximate reasoning. The defuzzifier is used to yield a crisp value from an inferred fuzzy value.

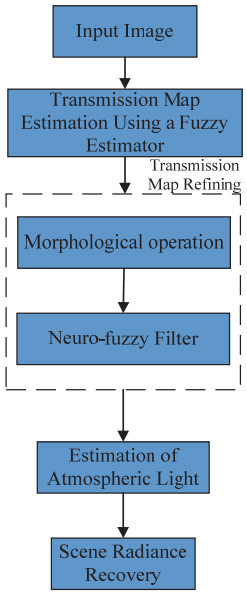

Fig. 2. Image dehazing process by using proposed hybrid method.

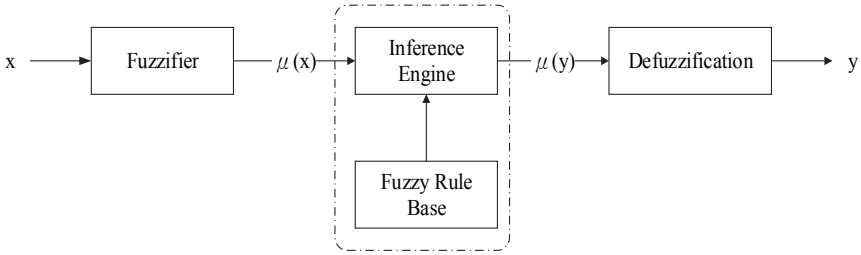

Fig. 3. Basic architecture of a fuzzy logic system.

Haze is a natural phenomenon resulting from light attenuation. When light penetrates through particles suspended in the air, the light attenuation varies according to the amounts and distribution of particles. Based on the above-mentioned physical hypothesis, the estimation of light attenuation is deemed as a nonlinear problem. In order to solve the nonlinear problem, an efficient fuzzy estimator is designed to estimate the transmission map based on the pre-observation of hazy and non-hazy images, as shown in Fig. 4.

First, the red-green-blue (RGB) of the input image is read and stored as single-channel images. A mask with a fixed size is then used to scan the RGB single-channel images. Meanwhile, the minimum pixel value for each block Ω is calculated as follows.

$$R_{\min} = \min_{i\in\Omega(x)} R_i,\ G_{\min} = \min_{i\in\Omega(x)} G_i,\ B_{\min} = \min_{i\in\Omega(x)} B_i \tag{3}$$

The minimum pixel value ($X_{\min}$) for each channel, obtained by using 7×7 mask size, is treated as the input variables (0~255) in the fuzzy logic system. The fuzzy estimator

proposed in this study comprises three inputs (*i.e.*, R_{min}, G_{min}, and B_{min}) and one output (*i.e.*, transmission map estimation). The membership functions of three inputs are shown in Fig. 5 (a), whereas the membership functions of one output are shown in Fig. 5 (b). The haze and haze-free images are achieved from the real scenes and internet. Based on the results of many experiments in haze images, if an area with the lower pixel value has a higher saturation color (*i.e.*, this is a haze-free area), the intensity of transmission map in this area tends to 1. An area with a medium pixel value is located between a haze-free area and a hazy area, and the transmission map intensity decreases as the pixel value increases. A high pixel value indicates that an area is haze or the sky. To prevent the lower saturation in hazy areas from influencing the image quality, the intensity of the transmission map approximates 0.

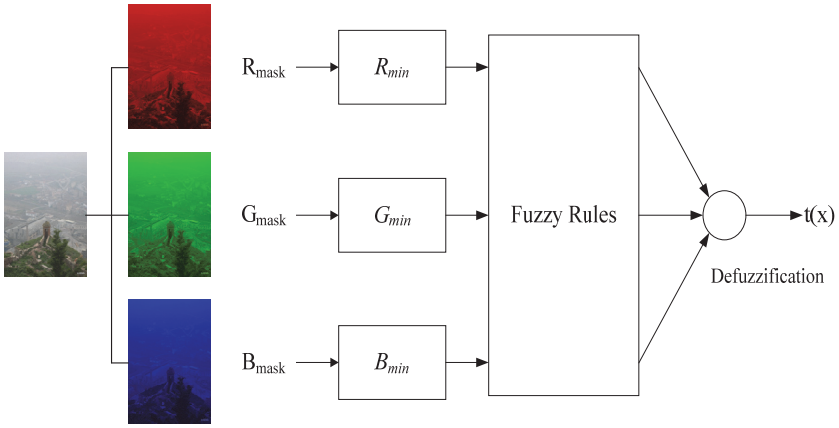

Fig. 4. Transmission map estimation using a fuzzy estimator.

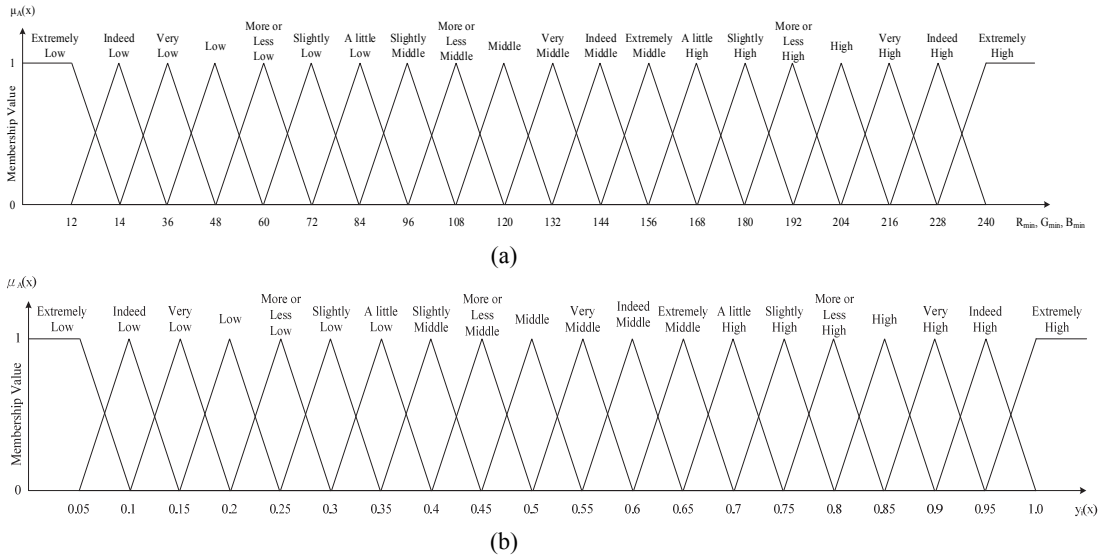

Fig. 5. Linguistic variables in the fuzzy rules for (a) each input; (b) each output.

The fuzzy rules of a fuzzy estimator are defined as follows:

Rule 1: IF ($R_{\min}$ is *Extremely Low* and $G_{\min}$ is *Extremely Low* and $B_{\min}$ is *Extremely Low*)
THEN (transmission map is *Extremely High*).
Rule 2: IF ($R_{\min}$ is *Extremely Low* and $G_{\min}$ is *Extremely Low* and $B_{\min}$ is *Indeed Low*)
THEN (transmission map is *Extremely High*).
Rule 3: IF ($R_{\min}$ is *Extremely Low* and $G_{\min}$ is *Indeed Low* and $B_{\min}$ is *Extremely Low*)
THEN (transmission map is *Extremely High*).
Rule 4: IF ($R_{\min}$ is *Extremely Low* and $G_{\min}$ is *Indeed Low* and $B_{\min}$ is *Indeed Low*)
THEN (transmission map is *Indeed High*).
Rule 5: IF ($R_{\min}$ is *Indeed Low* and $G_{\min}$ is *Extremely Low* and $B_{\min}$ is *Extremely Low*)
THEN (transmission map is *Extremely High*).
Rule 6: IF ($R_{\min}$ is *Indeed Low* and $G_{\min}$ is *Extremely Low* and $B_{\min}$ is *Indeed Low*)
THEN (transmission map is *Indeed High*).
Rule 7: IF ($R_{\min}$ is *Indeed Low* and $G_{\min}$ is *Indeed Low* and $B_{\min}$ is *Extremely Low*)
THEN (transmission map is *Indeed High*).
Rule 8: IF ($R_{\min}$ is *Indeed Low* and $G_{\min}$ is *Indeed Low* and $B_{\min}$ is *Indeed Low*)
THEN (transmission map is *Indeed High*).
:
Rule *n*: IF ($R_{\min}$ is *Extremely High* and $G_{\min}$ is *Extremely High* and $B_{\min}$ is *Extremely High*)
THEN (transmission map is Extremely Low).

Finally, to calculate the output of the fuzzy estimator, the Center of Area (COA) [29] is employed at the defuzzification step to estimate the transmission map;

$$t(x) = \frac{\sum_{i=1}^{n} (\pi_{j=1}^{m} \mu_A(x_j) \times y_i)}{\sum_{i=1}^{n} \pi_{j=1}^{m} \mu_A(x_j)}. \tag{4}$$

Where $\mu_A(x_j)$ is the membership degree of input and y_i is the consequent output of the ith fuzzy rule. Therefore, the transmission map $t(x)$ can be obtained by the proposed fuzzy estimator.

The size of the mask affects the quality of transmission map estimation. There is not any well-defined criterion to select the size of mask. Several researchers [7-11] try to evaluate transmission map estimation by using different sizes of the mask. Example will be given to explain the effect. For the original image shown in Fig. 6 (a), Figs. (b)-(d) show the estimates a transmission map using 1×1, 7×7, and 15×15 masks, respectively. Obviously, a smaller mask produces better quality of the transmission map image, as shown in Fig. 6 (e). No halation occurs during scene radiance recovery. Unfortunately, the color in this figure is over-saturation, which is not a desired representation of the original image. On the contrary, a larger mask recovers more natural color of the scene radiance; however, halation exists, as shown in Fig. 6 (g). With tolerable halation and natural color presentation, the scene radiance recovery effect of Fig. 6 (f) lies between that of Figs. 6 (e) and (g). Demonstrating the difference between these images, the image in Fig. 6 (f), which was obtained using a 7×7 mask, shows the transmission map estimation from an input hazy image. In this image, the halo artifacts appear to have been suppressed. Therefore, in this study, a 7×7 mask was adopted to balance the effect.

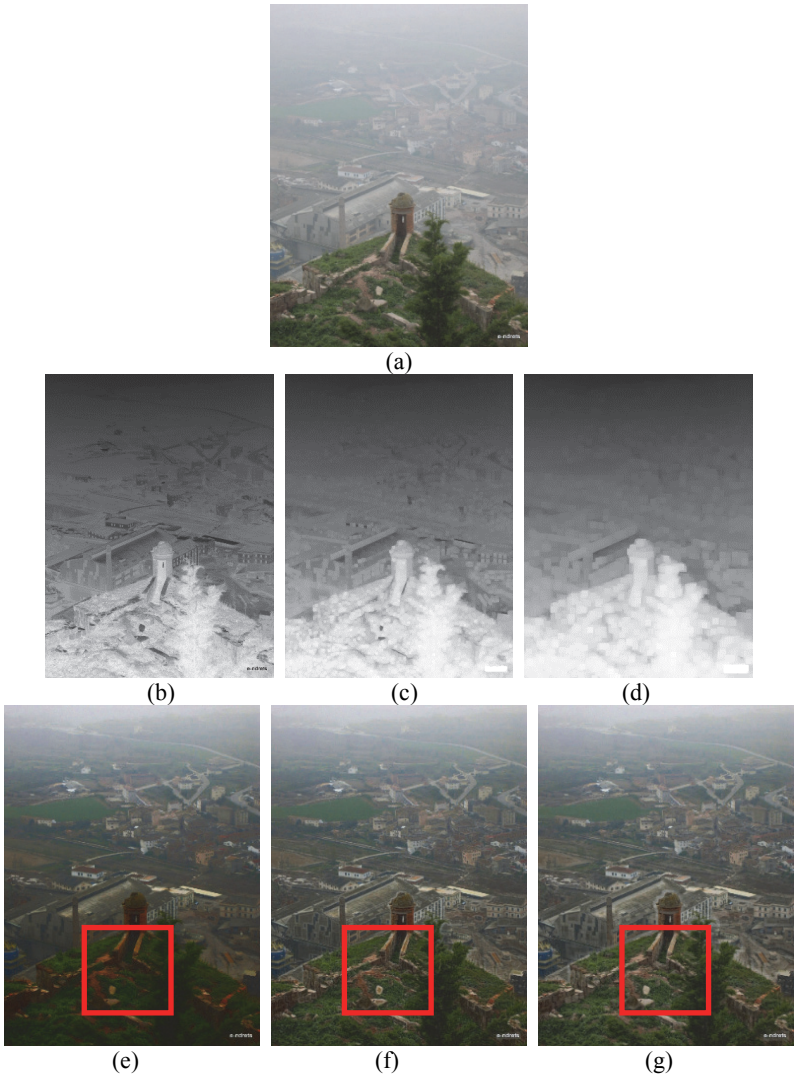

Fig. 6. The analysis of mask sizes; (a) Original image; (b)-(d) The estimates of transmission map with the mask sizes of 1×1, 7×7, and 15×15; (e)-(g) The corresponding scene radiance recoveries to (b)-(d).

3.2 Morphological Erosion

A mask is applied to estimate the transmission map, meaning that the local pixel transmission is the same as the surrounding area, resulting in block effect and halation during scene radiance recovery. The local light attenuation is different in actual environment, and in order to eliminate the halation, previous study [9] utilized the technique of refinement, which eliminating most of the halation. However, halation remains in some images, as shown in Fig. 7.

(a) (b) (c) (d)

Fig. 7. The halation (a) Original image; (b) Estimate of transmission map; (c) Refinement of transmission map; (d) Scene radiance recovery.

The refinement removes only some of the halation. The input of the fuzzy estimator is determined according to the masks in the transmission map. The difference between the images shows that larger masks enlarge the images, as shown in Fig. 8 (d), and this causes halation to occur after refinement. Fig. 8 (e) does not use the erosion method for halation removal. Hence, halo artifacts are clearly displayed around the object. By contrast, the halo artifacts can be suppressed by using the erosion method with a 7×7 erosion mask, as shown in Fig. 8 (f). Therefore, the present study adopted morphological erosion for halation removal.

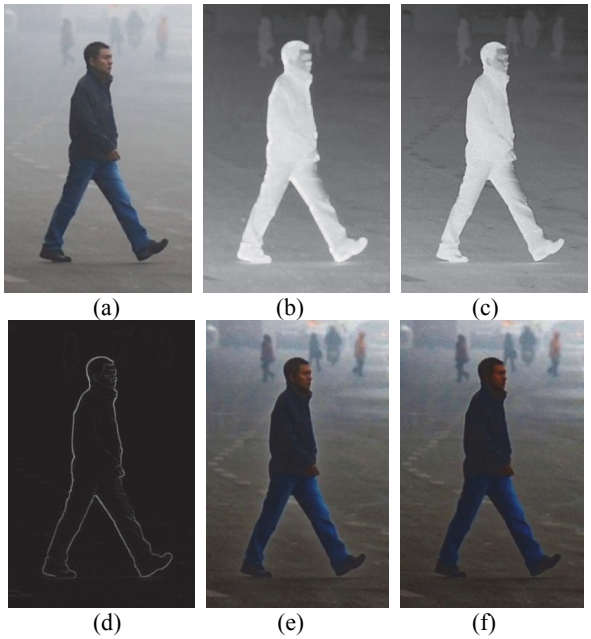

(a) (b) (c)

(d) (e) (f)

Fig. 8. Example of halation (a) Original image; (b)Transmission map estimation with 7×7 mask size; (c) Transmission map estimation with 1×1 mask size; (d) Results of the difference of images; (e) Halation removal without erosion method; (f) Halation removal with erosion method.

3.3 The Proposed Neuro-Fuzzy Filter

The proposed neuro-fuzzy filter (NFF) [25], which combines a neuro-fuzzy network and a functional link neural network (FLNN) [29], has been successfully applied in various fields, such as control, system identification, prediction, *etc.* Each fuzzy rule that corresponds to a FLNN consists of a functional expansion of input variables. The orthogonal polynomials and linearly independent functions are adopted as functional link neural network bases. The FLNN is a single layer neural structure capable of forming arbitrarily complex decision regions by generating nonlinear decision boundaries with nonlinear functional expansion. Moreover, the functional expansion is effectively used to increase the dimensionality of the input vector. Thus, the hyper-planes generated by the FLNN provide a good discrimination capability in input data space. The local properties of the consequent part in the NFF enable a nonlinear combination of input variables and approximate any continuous function more effectively. In [25], the experimental results show that the proposed NFF has a faster convergent speed and needs fewer fuzzy rules than other models. In this study, the proposed NFF will be applied for transmission map refinement and halation elimination.

The structure of neuro-fuzzy filter is presented in Fig. 9. The NFF realizes a fuzzy if-then rule.

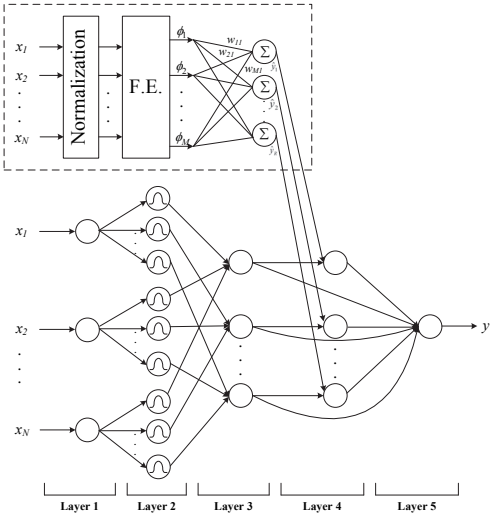

Fig. 9. Structure of the proposed neuro-fuzzy filter.

Rule-j: IF x_1 is A_{1j} and x_2 is A_{2j} … and x_i is A_{ij} … and x_N is A_{Nj}

$$\text{THEN } \hat{y}_j = \sum_{k=1}^{M} w_{kj}\phi_k = w_{1j}\phi_1 + w_{2j}\phi_2 + \ldots + w_{Mj}\phi_M \tag{5}$$

where x_i is the input variable and $\hat{y}_j$ is the local output variable; N is the number of input variables; M is the number of the basis trigonometric functions; w_{kj} represents the link

weight of a functional link neural network (FLNN); M is the number of basis function; A_{ij} represents the linguistic term of the precondition part with Gaussian membership function; and Rule-j is the jth fuzzy rule.

The following describes the operation functions of the nodes in each layer of the NFF. In which, $u^{(l)}$ represents the output of a node in the lth layer.

Each node directly transmits input values to the next following layer and executes no computation in Layer 1.

$$u_i^{(1)} = x_i \tag{6}$$

A proper Gaussian membership function is illustrated for each fuzzy set A_{ij}. The membership value in layer 2 is calculated as follows:

$$u_{ij}^{(2)} = \exp\left(-\frac{[u_i^{(1)} - m_{ij}]^2}{\sigma_{ij}^2} \right) \tag{7}$$

where m_{ij} and σ_{ij} are the mean and variance of the Gaussian membership function, respectively, of the jth term of the ith input variable x_i.

Nodes of a set in layer 2 feed one-dimensional membership degrees of the associated rule to nodes in layer 3. Each node performs a fuzzy AND operation on inputs. This study adopts an algebraic product operation. Consequently, the output is

$$u_j^{(3)} = \prod_i u_{ij}^{(2)} \tag{8}$$

where the $\prod_i u_{ij}^{(2)}$ of a rule node denotes the firing strength of its corresponding rule.

The nodes in layer 4 are named as consequent nodes. There are two input sources in layer 4. One is the output of layer 3, and the other is the output of a FLNN. For such a node,

$$u_j^{(4)} = u_j^{(3)} \cdot \sum_{k=1}^{M} w_{kj} \phi_k \tag{9}$$

where w_{kj} denotes the corresponding link weight of FLNN; ϕ_k represents the functional expansion of input variables; M is the number of basis functions, $M = 3 \times N$; N represents the number of input variables; and F.E. represents the functional expansion.

The output node in layer 5 integrates all of the actions recommended by layers 3 and 4 and acts as a defuzzifier with

$$y = u^{(5)} = \frac{\sum_{j=1}^{R} u_j^{(4)}}{\sum_{j=1}^{R} u_j^{(3)}} = \frac{\sum_{j=1}^{R} u_j^{(3)} \left(\sum_{k=1}^{M} w_{kj} \phi_k \right)}{\sum_{j=1}^{R} u_j^{(3)}} = \frac{\sum_{j=1}^{R} u_j^{(3)} \hat{y}_j}{\sum_{j=1}^{R} u_j^{(3)}} \tag{10}$$

where R is the number of fuzzy rules, and y is the output of the NFF.

The supervised learning back-propagation (BP) algorithm is used to adaptively adjust the link weights in the consequent part and the parameters of the membership func-

tions. The detailed derivation process of back-propagation algorithm is described in [25].

Recently, He *et al.* [9, 10] proposed the estimation of atmospheric light and transmission factor of a hazy image based on the dark channel prior. He *et al.* [10] adopted a guided filter to refine the transmission map to avoid the halo problem. A pseudocode of the guided filter [10] is shown as follows:

Guided Filter Algorithm
Input: filtering input image p, guidance image I, radius r, regularization ε
Output: filtering output q.

1: $mean_I = f_{mean}(I)$
$mean_p = f_{mean}(p)$
$corr_I = f_{mean}(I.*I)$
$corr_{Ip} = f_{mean}(I.*p)$
2: $var_I = corr_I - mean_{I.} * mean_I$
$cov_{Ip} = corr_{Ip} - mean_{I.} * mean_p$
3: $a = cov_{Ip./}(var_I + \varepsilon)$
$b = mean_p - a.* mean_I$
4: $mean_a = f_{mean}(a)$
$mean_b = f_{mean}(b)$
5: $q = mean_{a.} *I + mean_b$

In this algorithm, f_{mean} represents a mean filter with window radius r. The matrices $I.$, $p.$, and $a.$ represent the transpose of matrices I, p, and a. The abbreviations of correlation (corr), variance (var), and covariance (cov) indicate the intuitive meaning of these variables. This study presents the NFF to refine the transmission map and eliminate halation, as shown in Fig. 10. In order to refine the transmission map, the original image pixels and transmission map with erosion of morphological erosion are used as the inputs of the NFF, whereas the desired output of the NFF corresponds to the output of a guided filter [10] model. Because the computation time for the transmission map estimation and refinement of the original image in [9] is excessive, the present study replaced the guided filter with the trained NFF. During learning, the BP algorithm is continuously used to adjust the weights in the consequent part and the parameters of the membership functions and to reduce the error between the desired output $i_d(x)$ and the filter output $i(x)$. The output of NFF represents the transmission map of the original image and shows in Fig. 11 (b).

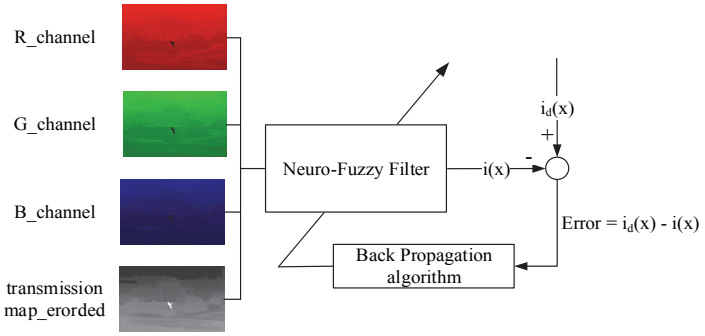

Fig. 10. The diagram of the proposed neuro-fuzzy filter.

(a) (b) (c)

Fig. 11. Results of (a) original image; (b) output of NFF; and (c) scene radiance recovery.

3.4 Mean Value Estimation of Atmospheric Light Vector

To overcome color cast, the atmospheric light used in this study is the surrounding natural light. Thus, the atmospheric light in the image comprises many pixels. Based on the result of the calculated atmospheric light image, pixel set x is formed by taking the top one percent brightest pixels in order to obtain their RGB values. The atmospheric color vector (ACV) is calculated as follows:

$$ACV^c = \frac{\sum_{pixel \in x} pixel^c}{|x|} \tag{11}$$

where $|x|$ is the number of the top one percent brightest pixels and c represents the RGB color channel.

In the scene radiance recovery step, the final dehazed image will be obtained using the following equation.

$$J(x) = \frac{I(x) - ACV^c}{\max(t_0, t(x))} + ACV^c \tag{12}$$

In Eq. (12), it is necessary to define the lower limit of the transmission factor t_o in order to reduce the noise of scene radiance recovery. In this study, t_o is set as 0.15, which can effectively reduce noise. Fig. 12 shows the results of scene radiance recovery using the brightest pixel and the mean value estimation of atmospheric light vector. Figs. 12 (b) and (c) show the image of atmospheric light using the brightest pixel as atmospheric light estimation and the result of scene radiance recovery, whereas Figs. 12 (d) and (e) show the image of atmospheric light using the mean value of the top one percent brightest pixels as atmospheric light estimation and the result of scene radiance recovery. The red color (*i.e.*, the street lamp and at the upper side) in Figs. 12 (b) and (d) represents the estimated area of atmospheric light. We can find that the proposed mean value of the top one percent brightest pixels as atmospheric light estimation has a better ability to discover the area of atmospheric light.

Finally, we summarize the proposed hybrid approach with the implementation steps in detail. The image dehazing process is shown as follows:

Step 1: Read an input image
Step 2: Use a fuzzy estimator for transmission map estimation (*i.e.*, Eq. (2))

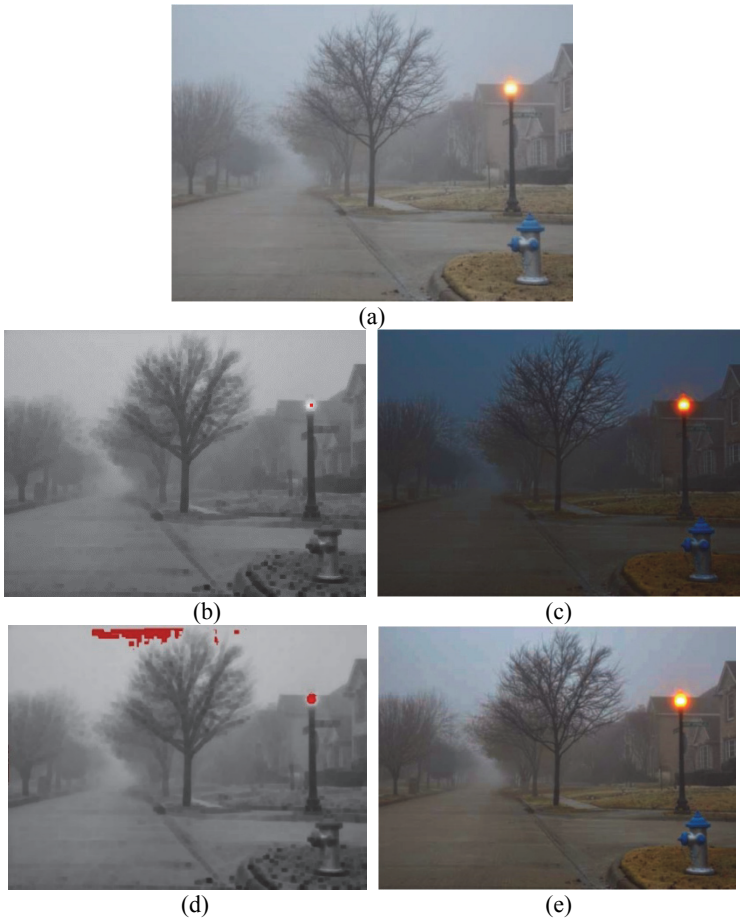

Fig. 12. (a) Original image; (b) The image of atmospheric light using the brightest pixel as atmospheric light estimation; (c) Scene radiance recovery of (b); (d) The image of atmospheric light using the mean value of the top one percent brightest pixels as atmospheric light estimation; (e) Scene radiance recovery of (d).

Step 3: Apply morphological erosion for the removal of halation around the object (*i.e.*, Subsection 3.2)
Step 4: Apply the NFF to eliminate the halation and preserve the edge of the object for transmission map refinement (*i.e.*, Fig. 11)
Step 5: Estimate the mean value of the atmospheric light vector (*i.e.*, Eq. (11))
Step 6: Obtain the scene radiance recovery (*i.e.*, Eq. (12))

4. EXPERIMENTAL RESULTS

In our experiments, we adopted the C programming language on a computer with a Pentium(R) i7-3770 CPU @3.20 GHz. The average size of the experimental image sample was approximately 600×400. This experiment was conducted to compare the results

of scene radiance recovery with different linguistic variables used for each input, and the selected most appropriate number of linguistic variables are compared with other dehazing methods. To demonstrate the effectiveness of the proposed dehazing method, both qualitative and quantitative performance comparisons are conducted in Section 4.2. In this study, the e and $\bar{r}$ quantitative assessment method proposed by Hautière *et al.* [28] is used. The parameters of the proposed dehazing method are set in Table 1.

Table 1. Parameter setting of the proposed dehazing method.

Parameter	Value
Input mask	7×7
Erosion mask	7×7
Iteration	50
Input dimension	4
Output dimension	1
Pixels of atmospheric light	1%
Transmission factor (t_0)	0.15

4.1 Algorithm Evaluation and Analysis

This study proposes a novel dehazing method in which an efficient fuzzy estimator is applied to estimate the transmission map, the atmospheric light image is calculated using a mean value estimate, and the proposed NFF is employed to optimize the transmission map refinement. After training the proposed NFF, six fuzzy rules are generated and shown as follows:

Rule 1: IF x_1 is μ(0.318830, –3.611479) and x_2 is μ(0.336451, 14.688882) and
x_3 is μ(–0.946811, –211.096424) and x_4 is μ(0.289905, –135.861459)
THEN $y = 0.856035x_1 + 0.173776\sin(\pi x_1)+0.132077\cos(\pi x_1)$
$–0.129642x_2+0.045836\sin(\pi x_2)–0.0005;46\cos(\pi x_2)$
$+0.340770x_3–0.039179\sin(\pi x_3)+0.149237\cos(\pi x_3)$
$+0.107190\, x_4–0.132514\, \sin(\pi x_4)+0.063590\cos(\pi x_4)$

Rule 2: IF x_1 is μ(0.005648, 0.189077) and x_2 is μ(0.743693, 0.191200) and
x_3 is μ(0.966295, 0.061953) and x_4 is μ(1.097528, –0.092159)
THEN $y = 0.627833x_1–0.687275\sin(\pi x_1)–0.495185\cos(\pi x_1)$
$+0.805106\, x_2–0.062883\, \sin(\pi x_2)+1.040078\cos(\pi x_2)$
$+0.582847x_3+0.362007\sin(\pi x_3)–0.108632\cos(\pi x_3)$
$+0.368671\, x_4+0.669236\sin(\pi x_4)+0.845034\, \cos(\pi x_4)$

Rule 3: IF x_1 is μ(–0.080694, 0.121793) and x_2 is μ(0.535196, 0.039421) and
x_3 is μ(0.550929, 0.139038) and x_4 is μ(7.383048, –166.800868)
THEN $y = 0.112023\, x_1+0.095491\sin(\pi x_1)+ 0.048169\, \cos(\pi x_1)$
$+0.270528\, x_2+0.754928\, \sin(\pi x_2)–0.332777\cos(\pi x_2)$
$–0.633098\, x_3+0.299237\sin(\pi x_3)+0.349629\cos(\pi x_3)$
$+0.791308\, x_4+0.056445\sin(\pi x_4)+0.501202\cos(\pi x_4)$

Rule 4: IF x_1 is μ(–0.113779, –0.071852) and x_2 is μ(0.573392, 0.071787) and
x_3 is μ(0.755576, 0.196972) and x_4 is μ(0.735493, 0.196823)
THEN $y = 0.670150\, x_1–0.256506\, \sin(\pi x_1)–0.545863\cos(\pi x_1)$

$$-0.495940x_2-0.560159\sin(\pi x_2)+0.446014\cos(\pi x_2)$$
$$+0.717507x_3+0.524792\sin(\pi x_3)+0.511702\cos(\pi x_3)$$
$$+0.986827x_4-0.223295\sin(\pi x_4)-0.962132\cos(\pi x_4)$$

Rule 5: IF x_1 is $\mu(-0.048975, 0.054404)$ and x_2 is $\mu(1.554979, -14.353817)$ and x_3 is $\mu(0.764134, 0.207305)$ and x_4 is $\mu(1.259776, 0.351388)$

THEN $y = 0.886521x_1+0.57521\sin(\pi x_1)+0.364946\cos(\pi x_1)$
$-0.251301x_2+0.085682\sin(\pi x_2)-0.644672\cos(\pi x_2)$
$-0.794236x_3-0.181070\sin(\pi x_3)+0.243473\cos(\pi x_3)$
$-0.127552x_4-0.434803\sin(\pi x_4)-0.708017\cos(\pi x_4)$

Rule 6: IF x_1 is $\mu(-0.139917, 0.063790)$ and x_2 is $\mu(0.320878, 0.449112)$ and x_3 is $\mu(0.888172, 1.592415)$ and x_4 is $\mu(0.677382, 0.182004)$

THEN $y = 0.839759x_1+0.484101\sin(\pi x_1)-0.703749\cos(\pi x_1)$
$+0.383820x_2-0.889731\sin(\pi x_2)-0.654569\cos(\pi x_2)$
$-0.444237x_3+0.547771\sin(\pi x_3)+0.735244\cos(\pi x_3)$
$-0.735744x_4+1.026695\sin(\pi x_4)-0.670007\cos(\pi x_4)$

Scene radiance recovery was tested with different numbers of linguistic variables in each input (*i.e.*, 5, 10, 20, and 30 linguistic variables). The results of each experiment approximate those shown in Fig. 13. Strictly speaking, the difference in Fig. 13 is only slight. A fuzzy estimator with five linguistic variables has some hazing effects and details that are partially fuzzy in the scene radiance recovery image, whereas the fuzzy estimator with 30 linguistic variables in each input outperformed all other estimators. In other words, using more linguistic variables in each input improves the dehazing results. However, the haze is not completely eliminated. When the light is attenuated naturally in a real environment, images with a slightly hazy effect appear normal.

(a) (b) (c) (d) (e)

Fig. 13. Results of different linguistic variables in each input; (a) Original image; (b) 5 linguistic variables; (c) 10 linguistic variables; (d) 20 linguistic variables; (e) 30 linguistic variables.

A fuzzy estimator with fewer linguistic variables in each input is inadequate for realizing favorable scene radiance recovery results, whereas a fuzzy estimator with more linguistic variables in each input causes noise or color casting. Based on our experimental results, a fuzzy estimator with 20 linguistic variables in each input is suggested. Therefore, the total 20*20*20 fuzzy rules are used.

4.2 Performance Comparison and Analysis

Because the evaluation of images is subjectively different from person to person, qualitative and quantitative comparison approaches were adopted to describe the effectiveness of the propose approach in treating four typical images. The qualitative comparisons are shown in Fig. 18. The restored image in Fig. 18 (g) shows that the scene radiance recovery performance is good. In [14], pixel-level fusion was achieved between the initial medium transmission and coarse medium transmission in transmission map refinement. When that approach is used, the sky is too bright and the edges of objects are too sharp, and artifacts such as white spots appear on objects such as cliffs and buildings. This makes restored images appear unusual.

The quantitative assessment, which has been widely adopted [8, 15, 16], consists of metric value (e) and the quality of the contrast in the visible edges ($\overline{r}$). The e metric is proportional to the visible edges in the restored image. Definitively, a higher value of e represents better results. The metric value is expressed as follows:

$$e = \frac{n_r - n_o}{n_o} \tag{14}$$

where n_o and n_r are the number of visible edges in the original image and the restored image, respectively.

The value of $\overline{r}$ denotes the quality of the contrast in the visible edges of the restored image. This quality is proportional to the gradient. In other words, the higher the value of $\overline{r}$ is, the better the contrast in the visible edges of the restored image will be. The quality of the contrast is expressed as follows:

$$\overline{r} = \exp\left[\frac{1}{n_r}\sum_{P_i \in \wp_r} \log r_i\right] \tag{15}$$

where $\wp_r$ is the set of visible edges in the restored image, P_i represents the ith where $\wp_r$ is the set of visible edges in the restored image, P_i represents the ith element of the corresponding set $\wp_r$, and r_i denotes the ith rate of the gradients between the original and restored images. Table 2 illustrates the quantitative assessment of four typical images with e and $\overline{r}$. As evidenced by the e values in Table 2, the proposed method can increase the contrast of visible edges. Although the methods of Tan [7] and Tarel [8] obtain the more favorable r_i values than the method proposed in the present study, the e metric values reported in [7, 8] methods are very low. Thus, the methods in [7, 8] cause over-saturation and chromatic aberration, as evidenced by the images. In addition, the r_i values obtained in previous studies [6, 9, 10, 12, 14] are similar to the one for the proposed method, but the e metric of the proposed method is more favorable.

Furthermore, this study also compared the average computation times reported by Fattal (35 seconds) [6], Tan (45 seconds) [7], Tarel and Hautière (8 seconds) [8], He *et al.* (20 seconds) [9], He *et al.* (7.4 seconds) [10], and the method proposed in the present study (7 seconds). The processing times for the methods in [12, 14] were not reported. Experimental results show that the computation time of our method is shorter than those of other methods. In our experiments, after the off-line training the proposed NFF (about five minutes), the learned six fuzzy rules in the proposed NFF are directly used to test these images. Thus, the off-line training time in the proposed method is ignored in the comparison of the average computation times.

5. CONCLUSIONS

This study proposes a hybrid method for effectively eliminating hazy effects from images to enhance their visual quality. During dehazing, the fuzzy estimator evaluates the variation in light attenuation. Furthermore, morphological erosion and the proposed NFF remove the halation. Finally, the mean value estimation of atmospheric light is applied to mitigate color casting. Experimental results show that the proposed method outperforms others in dehazing, halation removal, and color cast removal. In this study, we employed 20×20×20 fuzzy rules in the fuzzy estimator, which is an exceptionally high number of rules, rendering the method more difficult to implement compared with other methods. In future research, reducing the number of fuzzy rules will be crucial.

(a) (b) (c) (d) (e) (f) (g) (h)

Fig. 14. From left to right: (a) original images y01, y16, ny12, ny17 (from top to down); (b) Tan [7] algorithm results; (c) Fattal [6] algorithm results; (d) Kopf *et al.* [12] algorithm results; (e) Tarel *et al.* [8] algorithm results; (f) He *et al.* [10] algorithm results; (g) Liu *et al.* [14] algorithm results; and (h) The proposed method results.

Table 2. Performance comparisons of various methods.

Method \ Image	y01		y16		ny12		ny17	
	e	$\bar{r}$	e	$\bar{r}$	e	$\bar{r}$	e	$\bar{r}$
Tan [7]	0.08	2.28	–0.08	2.08	–0.14	2.34	–0.06	2.22
Fattal [6]	0.04	1.23	0.03	1.27	–0.06	1.32	–0.12	1.56
Kopf *et al.* [12]	0.09	1.62	–0.01	1.34	0.05	1.42	0.01	1.62
Tarel and Hautière [8]	0.02	2.09	–0.01	2.01	0.07	1.88	–0.01	1.87
He *et al.* [9]	0.08	1.33	0.06	1.42	0.06	1.42	0.01	1.65
He *et al.* [10]	0.133	1.20	0.14	1.30	0.06	1.20	0.04	1.26
Liu *et al.* [14]	0.11	1.66	0.09	1.61	0.07	1.62	0.04	1.69
Proposed	0.15	1.61	0.12	1.65	0.10	1.67	0.06	1.71

REFERENCES

1. Y. Y. Schechner, S. G. Narasimhan, and S. K. Nayar, "Instant dehazing of images using polarization," in *Proceedings of IEEE Computer Society Conference on Computer Vision and Pattern Recognition*, Vol. 1, 2001, pp. 325-332.
2. S. G. Narasimhan and S. K. Nayar, "Vision and the atmosphere," *International Journal of Computer Vision*, Vol. 48, 2002, pp. 233-254.
3. S. G. Narasimhan and S. K. Nayar, "Chromatic framework for vision in bad weather," in *Proceedings of IEEE Conference on Computer Vision and Pattern Recognition*, Vol. 1, 2000, pp. 598-605.
4. S. K. Nayar and S. G. Narasimhan, "Vision in bad weather," in *Proceedings of the 7th IEEE International Conference on Computer Vision*, Vol. 2, 1999, pp. 820-827.
5. S. Shwartz, E. Namer, and Y. Y. Schechner, "Blind haze separation," in *Proceedings of IEEE Computer Society Conference on Computer Vision and Pattern Recognition*, Vol. 2, 2006, pp. 1984-1991.
6. R. Fattal, "Single image dehazing," in *Proceedings of the 35th ACM International Conference and Exhibition on Computer Graphics and Interactive Techniques*, Vol. 27, 2008, pp. 1-8.
7. R. T. Tan, "Visibility in bad weather from a single image," in *Proceedings of IEEE Conference on Computer Vision and Pattern Recognition*, 2008, pp. 1-8.
8. J. P. Tarel and N. Hautiere, "Fast visibility restoration from a single color or gray level image," in *Proceedings of the 12th IEEE International Conference on Computer Vision*, 2009, pp. 2201-2208.
9. K. He, J. Sun, and X. Tang, "Single image haze removal using dark channel prior," *IEEE Transactions on Pattern Analysis and Machine Intelligence*, Vol. 33, 2011, pp. 2341-2353.
10. K. He, J. Sun, and X. Tang, "Guided image filtering," *IEEE Transactions on Pattern Analysis and Machine Intelligence*, Vol. 35, 2013, pp. 1397-1409.
11. G. F. Meng, Y. Wang, J. Duan, S. Xiang, and C. Pan, "Efficient image dehazing with boundary constraint and contextual regularization," in *Proceedings of IEEE International Conference on Computer Vision*, 2013, pp. 617-624.
12. J. Kopf, B. Neubert, B. Chen, M. Cohen, D. Cohen-Or, O. Deussen, M. Uyttendaele, and D. Lischinski, "Deep photo: Model-based photograph enhancement and view-

ing," *ACM Transactions on Graphics*, Vol. 27, 2008, pp. 1-10.
13. J. Long, Z. Shi, W. Tang, and C. Zang, "Single remote sensing image dehazing," *IEEE Geoscience and Remote Sensing Letters*, Vol. 11, 2014, pp. 59-63.
14. H. B. Liu, J. Yang, Z. P. Wu, and Q. N. Zhang, "Fast single image dehazing based on image fusion," *Journal of Electronic Imaging*, Vol. 24, 2015, pp. 013020-1–013020-10.
15. J. G. Wang, S. C. Tai, and C. J. Lin, "Image haze removal using a hybrid of fuzzy inference system and weighted estimation," *Journal of Electronic Imaging*, Vol. 24, 2015, pp. 033027-1–033027-13.
16. J. G. Wang, S. C. Tai, and C. J. Lin, "Transmission map estimation of weather degraded images using a hybrid of recurrent fuzzy CMAC and weighted strategy," *Optical Engineering*, Vol. 55, 2016, pp. 083104-1~083104-14.
17. D. van de Ville, M. Nachtegael, D. van der Weken, E. E. Kerre, W. Philips, and I. Lemahieu, "Noise reduction by fuzzy image filtering," *IEEE Transactions on Fuzzy Systems*, Vol. 11, 2003, pp. 429-436.
18. O. Mendoza, P. Melin, and G. Licea, "A hybrid approach for image recognition combining type-2 fuzzy logic, modular neural networks and the Sugeno integral," *Information Sciences*, Vol. 179, 2009, pp. 2078-2101.
19. D. L. Peng and T. J. Wu, "A generalized image enhancement algorithm using fuzzy sets and its application," in *Proceedings of IEEE Conference on Machine Learning and Cybernetics*, Vol. 2, 2002, pp. 820-823.
20. J. G. Daugman, "Complete discrete 2-D gabor transforms by neural networks for image analysis and compression," *IEEE Transactions on Acoustics*, *Speech and Signal Processing*, Vol. 36, 1988, pp. 1169-1179.
21. Y. T. Zhou, R. Chellappa, A. Vaid, and B. K. Jenkins, "Image restoration using a neural network," *IEEE Transactions on Acoustics*, *Speech and Signal Processing*, Vol. 36, 1988, pp. 1141-1151.
22. H. A. Rowley, S. Baluja, and T. Kanade, "Neural network-based face detection," *IEEE Transactions on Pattern Analysis and Machine Intelligence*, Vol. 20, 1998, pp. 23-38.
23. S. C. Kuo, C. J. Lin, and J. R. Liao, "3D reconstruction and face recognition using kernel-based ICA and neural networks," *Expert Systems with Applications*, Vol. 38, 2011, pp. 5406-5415.
24. I. Kanellopoulos and G. G. Wilkinson, "Strategies and best practice for neural network image classification," *International Journal of Remote Sensing*, Vol. 18, 1997, pp. 711-725.
25. C. H. Chen, C. J. Lin, and C. T. Lin, "A functional-link-based neuro-fuzzy network for nonlinear system control," *IEEE Transactions on Fuzzy Systems*, Vol. 16, 2008, pp. 1362-1378.
26. L. A. Zadeh, "Fuzzy Sets," *Information and Control*, Vol. 8, 1965, pp. 338-353.
27. J. Yen and R. Langari, *Fuzzy Logic: Intelligence*, *Control*, *and Information*, Prentice Hall, NJ, 1999.
28. N. Hautiere, J. P. Tarel, D. Aubert, and É. Dumont, "Blind contrast restoration assessment by gradient ratioing at visible edges," *Image Analysis & Stereology*, Vol. 27, 2008, pp. 87-95.

29. J. C. Patra, R. N. Pal, B. N. Chatterji, and G. Panda, "Identification of nonlinear dynamic systems using functional link artificial neural networks," *IEEE Transactions on Systems*, *Man*, *and Cybernetics Part B: Cybernetics*, Vol. 29, 1999, pp. 254-262.

Hsueh-Yi Lin (林學儀) received the M.S. degree in Computer Science from the Northrop University, California USA, in 1991. Currently, he is an Associate Professor of Computer Science and Information Engineering Department of National Chin-Yi University of Technology, Taichung County, Taiwan. His research interests are image processing, computer network, computational intelligence, and fuzzy theory.

Cheng-Jian Lin (林正堅) received the Ph.D. degree in Electrical and Control Engineering from the National Chiao-Tung University, Taiwan, in 1996. Currently, he is a Distinguished Professor of Computer Science and Information Engineering Department, National Chin-Yi University of Technology, Taichung County, Taiwan. His current research interests are computational intelligence, intelligent transportation system, intelligent control, image processing, bioinformatics, and Android/iPhone program design.

Mei-Ling Huang (黃美玲) received her M.S. and Ph.D. in Industrial Engineering from University of Wisconsin-Madison and National Chiao-Tung University. Now, she is affiliated with the Department of Industrial Engineering and Management in National Chin-Yi University of Technology. Her research interests include quality management, quality engineering, data mining, and medical assistant diagnosis.